Cellular pattern formation in circular domains

Antonio Palacios,[a] Gemunu H. Gunaratne,[b] and Michael Gorman[c]
Department of Physics, The University of Houston, Houston, Texas 77204

Kay A. Robbins[d]
Division of Computer Science, University of Texas at San Antonio, San Antonio, Texas 78249

(Received 7 April 1997; accepted for publication 24 June 1997)

An analysis of stationary and nonstationary cellular patterns observed in premixed flames on a circular, porous plug burner is presented. A phenomenological model is introduced, that exhibits patterns similar to the experimental states. The primary modes of the model are combinations of Fourier–Bessel functions, whose radial parts have neighboring zeros. This observation explains several features of patterns, such as the existence of concentric rings of cells and the weak coupling between rings. Properties of rotating rings of cells, including the existence of modulated rotations and heteroclinic cycles can be deduced using mode coupling. For nonstationary patterns, the modal decomposition of experimental data can be carried out using the Karhunen–Loéve (KL) analysis. Experimental states are used to demonstrate the possibility of using KL analysis to differentiate between uniform and nonuniform rotations. The methodology can be extended to study more complicated nonstationary patterns. In particular, it is shown how the complexity of ''hopping states'' can be unraveled through the analysis. © *1997 American Institute of Physics.* [S1054-1500(97)01103-8]

Recent studies of pattern formation on experimental systems and mathematical models have clearly demonstrated the existence of ''universal'' features that depend strongly on the nonlinearities of the physical system and the geometry of the domain. Motivated by the observation of novel stationary and nonstationary cellular states on a flame front, we develop a coherent scheme for the analysis of cellular patterns generated on a circular domain. The uniform flame front can bifurcate to a variety of cellular states depending on the size of the individual cells. The form of these primary modes are determined using data from experiments and also from the integration of a phenomenological model. It is demonstrated that apparently complicated dynamics can result from the coupling between a few principal modes.

I. INTRODUCTION

Flame patterns generated on a circular burner exhibit a wide array of complex spatiotemporal states with novel features. They include cells that exhibit uniform rotations,[1] intermittent motions[2] and chaotic dynamics.[3,4] Realistic modeling of the system combining the reaction-diffusion equations with the appropriate fluid dynamics would, in principle, provide a panoptic description of all observed states of the system. However, the capabilities for conducting this formidable computational task will not be available in the near future. In addition, the role played by the geometry of the system and intricate connections between distinct states are best studied in simplified models.

In this paper we demonstrate how a phenomenological model and bifurcation theory[5] can be used to understand certain aspects of cellular pattern formation on a circular flame front. Bifurcations from the uniform (flat) flame front lead to patterns of concentric cells through spontaneous symmetry breaking. The circular geometry suggests an expansion of the broken-symmetry states in a Fourier–Bessel series. In parameter domains where two or more distinct modes compete, their coupling can have subtle and interesting effects that can be described by the appropriate normal form theory.[6] Several properties of stationary and nonstationary cellular states of the flame front are explained as consequences of this analysis.

In the next section, we describe the experimental system, which consists of a circular burner that produces a combustion front from a uniformly flowing mixture of a fuel and air. For suitable control parameters the flame front consists of cellular states, such as that shown in Fig. 1(a). Observe that the aspect ratio (the size of the combustion front to that of the cells) is of the order of unity, so that the boundary conditions play a crucial role in the determination of the cellular structure. Figure 1(a) shows a state with two rings of different symmetries. The inner ring contains three cells (and has approximate D_3 symmetry) while the outer ring has eight cells (and is approximately D_8 invariant). The experiments also show many nonstationary states like rotating rings of cells,[1] hopping modes (where three cells rotate nonuniformly[2]) and ratcheting states (where two rings of cells move intermittently with different mean rotation rates).[4] The mode-coupling theory is expected to describe the

[a]Electronic mail: palacios@nomad44.laptop.uh.edu
[b]Electronic mail: gemunu@uh.edu
[c]Electronic mail: gorman@uh.edu
[d]Electronic mail: krobbins@runner.utsa.edu

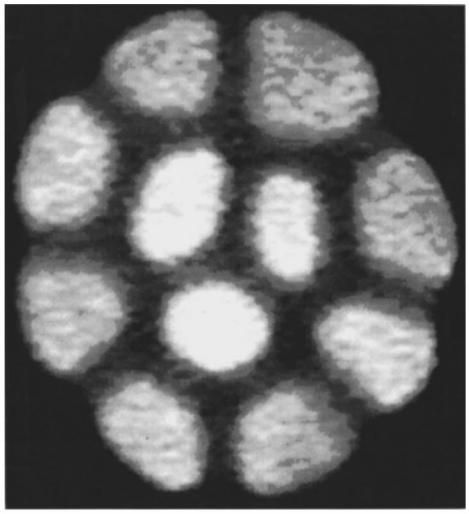

(a)

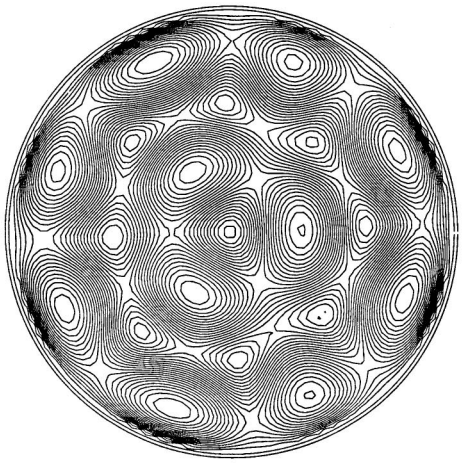

(b)

FIG. 1. (a) Stationary pattern of cells from the experiments, and (b) the analogous pattern from the integration of the model (3.1). Notice that the pattern consists of two rings with approximate symmetries D_3 and D_8.

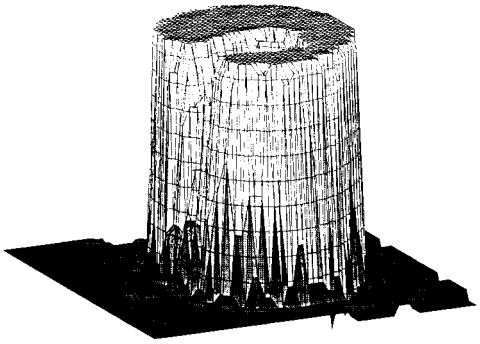

(a)

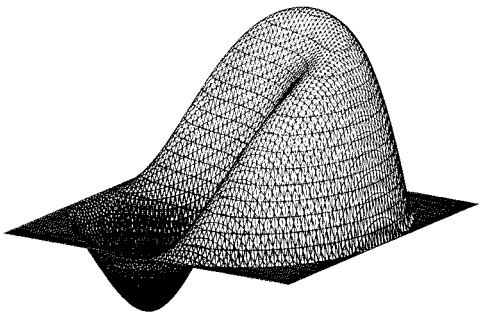

(b)

FIG. 2. (a) The intensity of a single-cell rotating state, and (b) the corresponding numerically generated state. The setting of the video camera required to view the cellular flames leads to a saturation of the intensity. Consequently, the experimental data need to be filtered prior to a modal analysis.

mechanisms for the generation of these states.

Figure 2(a) shows the intensity of a single rotating cell recorded on a video tape. A suitable modal decomposition of the state would lead to an understanding of the cell shape and the origin of the motion. The preliminary analysis is carried out on a numerically generated pattern. In Section III, a phenomenological model is presented to study the characteristics of cellular patterns[7] in a circular domain. The equations of the model are constructed with terms that describe the dominant physical mechanisms of the reaction and diffusion of a single species. The model is not meant to be a ''realistic'' description of the combustion processes (a premixed flame front contains many species, has heat loss to the burner, and produces a modification of the flow field), and can be integrated in polar coordinates using computationally efficient algorithms. Figure 1(b) shows contours of a stationary state from the model analogous to Fig. 1(a), while Fig. 2(b) shows the intensity of a single cell rotating state.

Dirichlet boundary conditions chosen for the phenomenological model suggest that the destabilization of the uniform state leads to a state whose intensity is proportional to a Fourier–Bessel (FB) function.[8] Linear and nonlinear stability analysis of this bifurcation is given in Section III. It is found that the primary bifurcations are subcritical. In Section IV, examples are presented that show how the subcriticality of the primary bifurcations and proximity of certain zeros of the Bessel functions can lead to states consisting of rings of cells.

Several experimental manifestations of the mode-coupling theory are provided in the remainder of the paper. In Section V, we present examples of rotating cells both from the experiment and the model. The Fourier–Bessel expansion of a single rotating cell demonstrates the existence of two leading FB modes whose (azimuthal) frequencies are in a ratio 1:2. The results from the numerical integration

exhibit cellular states which rotate uniformly as well as those that rotate nonuniformly. In addition, dynamical states that move on a heteroclinic cycle between a pair of two-cell states related by symmetry are presented and analyzed.

The existence of nonuniform rotating states and heteroclinic cycles was predicted by the normal form theory[9–11] when the primary bifurcations are supercritical. Our results suggest that the bifurcation sets corresponding to subcritical and supercritical bifurcations are similar. In the Appendix we present the normal form theory which corresponds to the case when the bifurcations to pure modes (i.e., Fourier–Bessel modes) are degenerate. The bifurcation diagram will be structurally stable under the unfolding of the degeneracy, thus explaining the similarity of the subcritical and supercritical cases.

In Section VI, we argue that the Karhunen–Loéve (KL) analysis can be used for the modal decomposition of nonstationary patterns on the flame front. It is used to differentiate between experimental states with uniform and nonuniform rotations. It is further argued that the KL decomposition can be used to eliminate higher dimensional effects from experimental data, thus allowing a direct check of the effects of mode coupling. As shown through several examples, the modal decomposition of these spatiotemporal states unravels their complexity and leads to the deduction of the appropriate normal form equations.

In the concluding section the methodology introduced here is used to analyze more complex dynamical states on the circular domain. Modal decompositions of ''hopping states'' provide the ''primary'' modes necessary for their existence, and demonstrate the need for studying mode couplings that do not appear naturally in one-dimensional problems.

II. THE EXPERIMENTAL SYSTEM

The experiments are conducted on a circular porous plug burner mounted in a combustion chamber kept at a pressure of 0.3–0.5 atm. The fuel and air are mixed prior to their entrance into the porous medium.[1] The uniform velocity field produces a flat flame front, a circular luminous disk, 5.62 cm in diameter and 0.5 mm thick, that sits 5 mm above the porous plug. The pressure, flow rate and fuel/oxidizer ratio are controlled to within 0.1%. A Dage-MTI charge-coupled device camera is mounted either vertically on the top of the combustion chamber or horizontally in the plane of the flame to record the dynamics on videotape.

Beyond a critical value of a control parameter, the flame front curves (locally), forming patterns of concentric rings of brighter (hotter) cells whose boundaries are demarked by darker (cooler) cusps and folds. These cusps extend about 5 mm further from the porous plug. In a typical experiment different patterns are selected by varying the flow rate and the equivalence ratio. Variations in the pressure are made to adjust the range of the number of cells. For example, single rings of cells are stable at 0.3 atm, but not at 0.5 atm. Changing the fuel can lead to additional patterns; ratcheting[4] and hopping motions[2] are found in isobutane-air mixtures but not in propane-air mixtures.

The distinctive feature of the patterns which form in premixed flames on a circular porous plug burner is the complex sequence of bifurcations from ordered patterns of concentric rings of cells to nonstationary patterns in which the rings of cells move collectively in an intricate manner. In rotating states, asymmetrically shaped cells rotate at a rate of approximately 100 deg/s. In hopping states individual cells sequentially make abrupt changes in their angular positions (6 Hz), while in ratcheting states one or more rings of (apparently) symmetric cells drift slowly (1 deg/s) except for intermittent jumps. These motions have only been observed in this system. In addition, the ordered states are unique among pattern-forming systems in that the boundaries between the cells exhibit small amplitude chaotic oscillations about their equilibrium positions. *A priori*, the description of these motions requires high accuracy measurements of the positions and shapes of the cells in each frame.

The height of the flame front is seen to be at a constant height at the boundary, except along a small length between the cells of the outer ring where it extends slightly further. This observation suggests the use of Dirichlet boundary conditions (as an approximation) on the model equation introduced in the next section. A co-flow of inert nitrogen gas can be sent through an annular disk surrounding the porous plug to reduce the shear between the premixed gas and the ambient vacuum. However, this co-flow has never produced an observable change on the dynamic states. In some experiments the cellular flame front does not completely fill the area of the porous plug, leaving a substantial region of unreacted premixed gas which then effectively acts as a weak co-flow. Occasionally, the edge of the flame front is seen to curl upward slightly. There is no evidence that either of these characteristics has any appreciable effect on the dynamics.

III. THE PHENOMENOLOGICAL MODEL

The aim of this work is an understanding of ''characteristic'' aspects of cellular patterns generated on circular domains. In particular, we wish to explain why the cellular states consist of rings of cells and to determine mechanisms through which nonstationary states are generated. We would also like an explanation of the weak (but nonzero) interaction between distinct rings of cells. The underlying suggestion is that these features arise primarily from spontaneous symmetry breaking and the geometry rather than from the specific physical mechanisms that govern the flame front.

The Kuramoto–Sivashinsky (KS)[12] equation is the simplest model of the thermodiffusive instability. It is derived by making a series of simplifying approximations of diffusion equations for two variables (chemical species and heat) coupled to fluid equations, and it captures qualitative features of cellular flames in extended domains.[13,14] To preserve the $O(2)$ invariance of the system, the integration has to be carried out in polar coordinates. The difficulty of integrating the KS equation in polar coordinates prevents us from using it for our study.

The phenomenological model used is a modification of the ''Brusselator'' (expanded about its uniform solution).[15] It describes the evolution of two coupled, diffusive spatiotemporal fields $u(\mathbf{x},t)$ and $v(\mathbf{x},t)$ through

$$\begin{aligned}\partial_t u &= \kappa_1 \nabla^2 u + (B-1)u + A^2 v - \eta u^3 - \nu_1 (\nabla u)^2, \\ \partial_t v &= \kappa_2 \nabla^2 v - Bu - A^2 v - \eta v^3 - \nu_2 (\nabla v)^2.\end{aligned} \tag{3.1}$$

The parameters κ_1 and κ_2 are the *diffusion coefficients* of the two fields which are coupled linearly. The cubic terms control the growth of the linearly unstable modes, while the nonlinear gradient terms render the model nonvariational. The form of the latter is similar to the nonlinear term of the KS equation, where it appears as a consequence of the curvature of the flame front.[13] The shape of the boundary of the flame front (discussed in Section II) motivates the imposition of Dirichlet boundary conditions on the fields $u(\mathbf{x},t)$ and $v(\mathbf{x},t)$. We do not believe that the results of the numerical studies discussed here depend on this choice.

In order to retain the rotational invariance of the system, we carry out the numerical integration in polar coordinates (r,ϕ). The form of the Laplacian, $\nabla^2 = \partial_{rr} + r^{-1}\partial_r + r^{-2}\partial_{\phi\phi}$ produces a (coordinate) singularity at the origin, which is avoided by partitioning each diameter into an even number of equally spaced lattice points. The numerical integration is carried out semi-implicitly through an Alternating Direction Implicit (ADI) algorithm in (r,ϕ) coordinates[16]. Each nonlinear term $N[u(\mathbf{x},t),v(\mathbf{x},t)]$ is expanded to linear order in $\delta u = u(\mathbf{x},t+\delta t) - u(\mathbf{x},t)$ and $\delta v = v(\mathbf{x},t+\delta t) - v(\mathbf{x},t)$, thus linearizing the equations in $u(\mathbf{x},t+\delta t)$ and $v(\mathbf{x},t+\delta t)$. Each step of the integration is carried out first along the diameter and then azimuthally, with a time step δt $(=0.05)$ small enough to justify the truncation of the expansion of nonlinear terms. For several states it was checked that the results are unchanged with smaller time steps. The numerical algorithm fails in the case of the Kuramoto–Sivashinsky equation due to the existence of the term $\nabla^4 u$, which when expanded in polar coordinates gives terms with cross derivatives such as $\partial_{rr\theta\theta} u$. In our numerical integrations, the ADI algorithm was seen to develop divergences at the origin when such terms are included.

Figures 1(b) and 4(b) show stationary states generated through the integration of the model. These are similar to the experimental patterns shown in Figs. 1(a) and 4(a). As shown later, we are also able to reproduce several nonstationary states that are analogous to experimentally observed patterns.

Although one would expect to obtain nonstationary states by using any nonvariational model [such as replacing the quadratic terms with $\pm u(\mathbf{x},t)v(\mathbf{x},t)$], we have only succeeded in doing so with the inclusion of the nonlinear gradient terms. This is particularly unfortunate, since the absence of the gradient terms would have allowed the reduction of Eq. (3.1) to a set of ordinary differential equations for the dynamics of Fourier–Bessel coefficients. The presence of the nonlinear gradient terms result in the coupling of a large number of FB modes and prevents the reduction of Eq. (3.1) to the set of ordinary differential equations. It is possible that the mode mixing implied by the presence of gradient terms and the Dirichlet boundary conditions plays a significant role in generating the nonstationary states.

A. Linear stability analysis

A smooth field $u(\mathbf{x},t)$ vanishing on the boundary of a circular domain of radius R can be expanded in a Fourier–Bessel series as

$$u(\mathbf{x},t) = \sum_{n,m} z_{nm}(t)\Psi_{nm}(r,\phi) + \text{c.c.}, \tag{3.2}$$

where $\Psi_{nm}(r,\phi) = J_n(\alpha_{nm} r/R)e^{in\phi}$, $(m \geq 0$ and $n > 0)$ and c.c. denotes the complex conjugate.[17] Here $J_n(r)$ is the nth order Bessel function of the first kind and α_{nm} is its mth nontrivial zero. z_{nm} are complex coefficients, save for z_{0m} which are real. The orthonormality and completeness of the functions $\{\Psi_{nm}: n \geq 0,\ m \geq 1\}$ gives

$$z_{nm} = \frac{1}{\pi R^2 J_{n+1}^2(\alpha_{nm})} \int_0^{2\pi} \int_0^R r u(r,\phi) \overline{\Psi}_{nm}(r,\phi)\, d\phi\, dr, \tag{3.3}$$

with the proviso that the coefficients are half of the value given when $n = 0$.

Thus the uniform state $(u,v) = (0,0)$ is stable if all perturbations of the type $(\delta u, \delta v)\Psi_{nm}$ decay. The marginal stability corresponds to those parameters when (at least) one such perturbation is marginal. Using $\nabla^2 \Psi_{nm} = -(\alpha_{nm}/R)^2 \Psi_{nm}$, and substituting in Eq. (3.1) gives

$$\frac{\partial}{\partial t}\begin{pmatrix} \delta u(t) \\ \delta v(t) \end{pmatrix} = \begin{pmatrix} m_{11} & m_{12} \\ m_{21} & m_{22} \end{pmatrix}\begin{pmatrix} \delta u(t) \\ \delta v(t) \end{pmatrix}, \tag{3.4}$$

where $m_{11} = B - 1 - \kappa_1(\alpha_{nm}/R)^2$, $m_{12} = A^2$, $m_{21} = -B$ and $m_{22} = -A^2 - \kappa_2(\alpha_{nm}/R)^2$.[5] The uniform state destabilizes to $\Psi_{nm}(r,\phi)$ beyond the curve

$$B_{nm}^M = 1 + \frac{\kappa_1}{\kappa_2}A^2 + \kappa_1\left(\frac{\alpha_{nm}}{R}\right)^2 + \frac{A^2}{\kappa_2}\left(\frac{R}{\alpha_{nm}}\right)^2. \tag{3.5}$$

For a given value of A, it reaches a minimum of

$$B_0 = 1 + \frac{\kappa_1}{\kappa_2}A^2 + 2A\sqrt{\frac{\kappa_1}{\kappa_2}} \tag{3.6}$$

at a radius $R_{nm} = \alpha_{nm}(\kappa_1\kappa_2/A^2)^{1/4}$. The results presented in this paper are evaluated with fixed values of $\kappa_1 = 0.2$, $\kappa_2 = 2.0$ and $A = 5.0$. B and R are used as the control parameters. The marginal stability curves of the trivial state to several Fourier–Bessel modes are shown in Fig. 3.

B. Nonlinear stability analysis

For parameters considered in the paper, it is found that the bifurcations from the uniform state to the FB modes are subcritical. The following calculation for the instability to Ψ_{11} supports this observation. The presence of the quadratic (gradient) term implies that we need to expand the fields (u,v) as

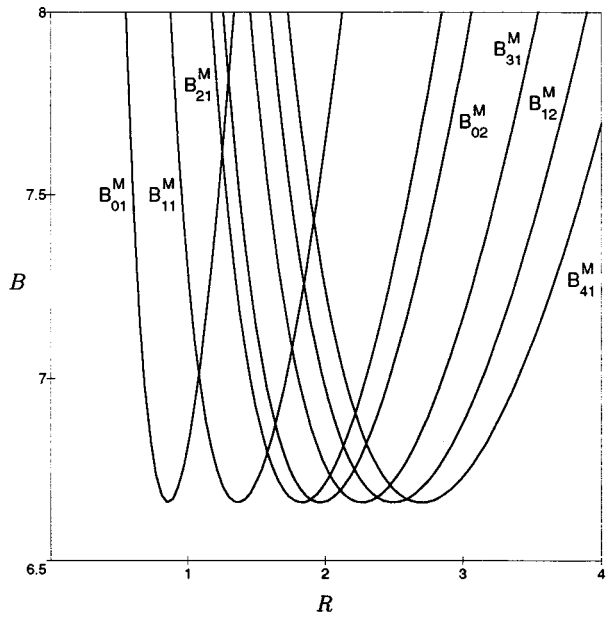

FIG. 3. Marginal stability curves along which the uniform state $(u,v)=(0,0)$ of (3.1) destabilizes to the Fourier–Bessel modes Ψ_{nm}. The curves are evaluated for fixed values of $\kappa_1=0.2$, $\kappa_2=2.0$ and $A=5.0$. B and the radius of the domain R are used as control parameters.

$$u(\mathbf{x},t)=u_1\Psi_{11}+u_2\Psi_{21}+\text{c.c.},$$
$$v(\mathbf{x},t)=v_1\Psi_{11}+v_2\Psi_{21}+\text{c.c.} \tag{3.7}$$

This form for the fields will be substituted in Eq. (3.1) and we will study its equilibrium by projecting onto the directions Ψ_{11} and Ψ_{21}. In order to complete the calculation we write $(\nabla u)^2=\gamma_1 u_2\overline{u}_1\Psi_{11}+\gamma_2 u_1^2\Psi_{21}\ldots$, and a similar expression for $(\nabla v)^2$.[18] Substituting these in Eq. (3.1) and projecting gives up to quadratic order in u_1, u_2, v_1 and v_2,

$$\begin{aligned} &m_{11}u_1+m_{12}v_1-\nu_1\gamma_1 u_2\overline{u}_1=0,\\ &m_{11}u_2+m_{12}v_2-\nu_1\gamma_2 u_1^2=0,\\ &m_{21}u_1+m_{22}v_1+\nu_2\gamma_1 v_2\overline{v}_1=0,\\ &m_{21}u_2+m_{22}v_2+\nu_2\gamma_2 v_1^2=0. \end{aligned} \tag{3.8}$$

It follows that the state is created along the marginal stability curve $B^M_{nm}(R)$. Writing $B=B^M_{nm}+\delta B$, Eq. (3.1) can be reduced to give

$$\delta B=c|u_1|^2, \tag{3.9}$$

where the prefactor c is negative for parameters considered in the paper. Thus small amplitude solutions to Eq. 3.1 exist when $\delta B<0$, and hence the bifurcations from the trivial states are subcritical. Figure 7 shows the bifurcations to the modes Ψ_{11} and Ψ_{21} which were obtained through the numerical integration of Eq. (3.1). A significant implication of the subcriticality is that the (observable) bifurcating states have finite amplitudes. Consequently, the nonlinear terms are crucial to determine the form of nontrivial states.

IV. ORDERED CELLULAR STATES

The discussion of the last section suggests that primary bifurcations from the uniform state lead to modes that are proportional to the Fourier–Bessel functions. This appears to be the case in some of the single ring flame patterns. Multiple ring Fourier–Bessel modes have also been observed in patterns from the Faraday experiments.[19,20] In this section we suggest, through examples, possible reasons for the conspicuous absence of the multiple ringed FB states (such as Ψ_{63}) in the flame patterns.

The presence of the nonlinear gradient terms and the imposition of Dirichlet boundary conditions imply that pure FB modes cannot be solutions of the phenomenological model (3.1) because all terms except the gradients vanish at the boundary of the domain. Consequently, solutions to the model equations will have to be combinations of FB modes, whose gradient vanishes at the boundary. The existence of cellular states can be traced to the proximity of certain roots of the FB functions, as we demonstrate through examples. The three ring cellular state shown in Fig. 4(a) can be approximated by a combination of the modes $\Psi_{12,1}$, Ψ_{63}, and Ψ_{06}. Observe the proximity of $\alpha_{12,1}$, α_{63}, and α_{06} allow these modes to be simultaneously excited. The subcriticality of the primary bifurcations, which imply the finiteness of the amplitudes, coupled with the necessity for the gradients of the fields to vanish at the boundary, make it imperative that such a combination of modes be excited.

As a second example we give the modal decomposition of the two-ring pattern with rings of three (3) and eight (8) cells, see Fig. 1. The two rings have distinct symmetries, and hence can be separated as follows. Fourier–Bessel decomposition of the state shows that the largest amplitudes correspond to modes with Ψ_{nm} with $m=0,3,6,8,9$, and 16. Combining the modes with $m=3,6,9$ gives the inner ring of cells, while the sum of modes with $m=8,16$ provide the outer ring. Figure 5 shows the results of the decomposition, and leads to an interesting observation. The intensity of each combination of modes is small outside of the corresponding ring. This feature may explain why the rings of cells are weakly coupled to each other in the nonstationary states.

V. NONSTATIONARY STATES: ROTATING RINGS OF CELLS

The utility of modal decomposition for the study of nonstationary states can be demonstrated through the analysis of a rotating ring of cells. Evidence for the existence of additional nonstationary states, predicted by the normal form theory, is given. It is known from experimental studies of one-dimensional systems that cellular patterns on interfaces drift when the cells are not invariant under reflections.[21] Theoretical analyses show how the asymmetry, which results from the coupling of modes with a wave-vector ratio 1:2, leads to drift modes.[9,10,22] These results have not been checked in geometries beyond (essentially) one-dimensional systems.

Figure 6 shows three pairs of patterns from the flame front. The stationary patterns in Figs. 6(a), 6(c) and 6(e) have

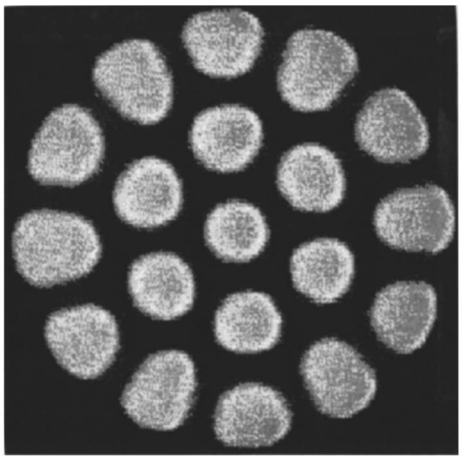

(a)

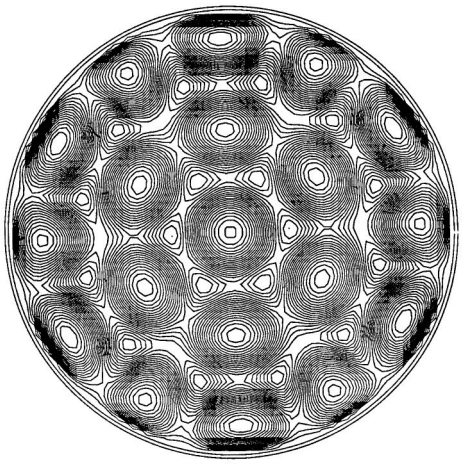

(b)

FIG. 4. Stationary cellular patterns generated in the (a) experiment and (b) the model, which have similar characteristics. In Section IV, we suggest a mechanism by which such cellular states (as opposed to pure Fourier–Bessel modes) can be formed.

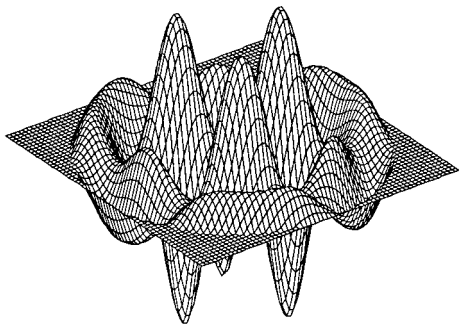

(a)

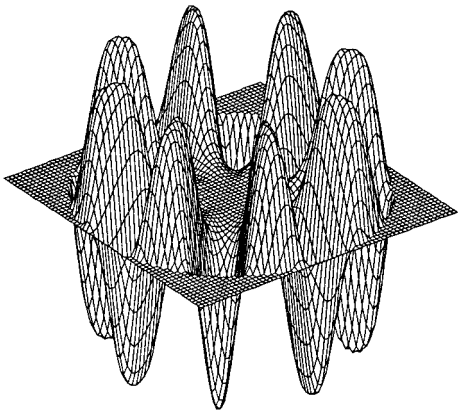

(b)

FIG. 5. The (a) inner and (b) outer ring of the state shown in Fig. 1(b). The rings are separated via a FB expansion as described in the text. Observe that the intensity of the field outside of the rings is small. This may explain why the interaction between rings is small in nonstationary patterns, such as the ratcheting states.

the same number of cells in each ring as their rotating counterparts shown in Figs. 6(b), 6(d) and 6(f), respectively. The rings shown in Figs. 6(b) and 6(d) are both rotating in a clockwise direction. In Fig. 6(f) the outer ring is fixed and the inner ring rotates in a counter-clockwise direction. The rotation of a ring at given control parameters can be either clockwise or counter-clockwise depending on the initial conditions. The crucial observations are that the cells in each rotating ring have lost their chiral symmetry,[7] and that the direction of rotation depends on the sense of the asymmetry. Fourier–Bessel decomposition of these states demonstrates that the asymmetry is produced by the phase difference of the modes. The blurring created by the rotation does not contribute to the observed asymmetry of the cells. These observations reinforce the relationship between the geometry (chiral asymmetry) of cells and the dynamics (rotation) of rings of cells.

We choose to study a single cell, the analysis of which captures many essential features of the rotating cellular patterns. Figure 7 shows the parameter space in the neighborhood of the mode coupling between Ψ_{11} and Ψ_{21}. The primary bifurcations to each pure mode are subcritical, as expected from the analysis of Section III. The shaded region to the left of the stability domain of Ψ_{21} contains several distinct nonstationary states. The first bifurcation (on moving right) occurs along the left edge of the shaded domain. It leads to a single uniformly rotating cell, which undergoes a Hopf bifurcation to a state whose angular velocity (as well as shape) is periodic. The final bifurcation, which occurs close to the right edge of the shaded region leads to a heteroclinic cycle between a pair of two-cell states which are at right angles to each other.

Rotating states of a single cell obtained from the numerical integration of Eq. (3.1) are presented in Fig. 8 along with the analogous experimental states. The chiral asymmetry is demonstrated by contrasting Fig. 8(a) with Fig. 8(b) and also Fig. 8(c) with Fig. 8(d). The computed and experimental cell shapes are similar as seen by comparing Fig. 8(a) and Fig.

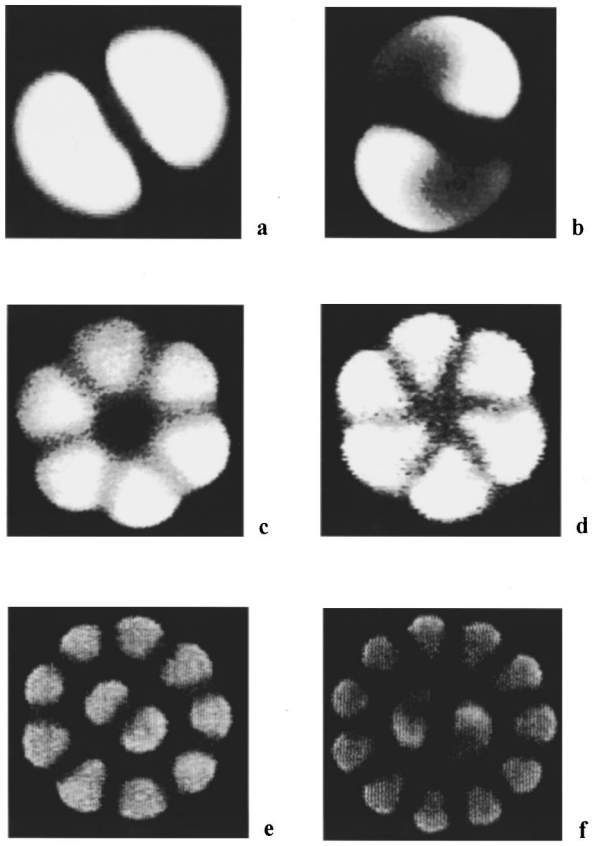

FIG. 6. Six cellular patterns generated on a circular flame front: (a) and (c) show stationary rings of two and six cells, respectively; (b) shows a ring of two cells, while (d) shows a ring of six cells, both rotating clockwise; (e) and (f) are states with a fixed outer ring and an inner ring of two cells. The cells in the inner ring of (e) are stationary, while those of (f) rotate counterclockwise. Observe that cells belonging to the stationary rings are chirally symmetric, while those of the rotating rings are not.

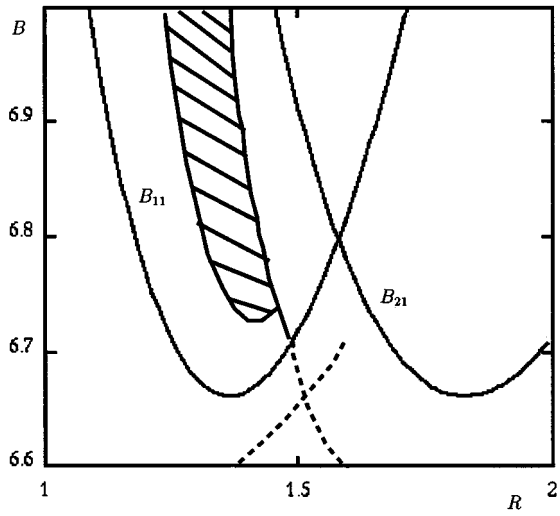

FIG. 7. Parameter space in the neighborhood of the mode-coupling between Ψ_{11} and Ψ_{21}. Observe that the primary bifurcation to each pure mode is subcritical. The shaded region to the left of the stability domain of Ψ_{21} contains several distinct nonstationary states. The first bifurcation (on moving right) leads to a single uniformly rotating cell, which experiences a Hopf bifurcation to a state whose angular velocity (as well as the shape) is periodic. The final bifurcation occurs close to the right end of the shaded region, and leads to a heteroclinic cycle between a pair of two-cell states related by symmetry.

8(c), and also Fig. 8(b) and Fig. 8(d). The Fourier–Bessel expansion of the rotating cell confirms that the modes with largest amplitude are Ψ_{01}, Ψ_{11} and Ψ_{21}. The real coefficients z_{0m} are constants of the motion. The amplitude and phase of the coefficients z_{11} and z_{21}, shown in Fig. 9, indicate that the state undergoes uniform rotation.

The presence of the nonlinear gradient term and the vanishing of the field at the boundary require the existence of secondary FB modes that are ''slaved'' to these primary modes. The behavior of their coefficients is similar to that of the corresponding primary mode. Thus, for the state shown in Fig. 8(a) the amplitude of coefficients z_{12}, z_{13}, etc., will be constant, and their phase will have the same slope as that of z_{11}.

In addition to the uniformly rotating states, the normal form analysis predicts the existence of nonuniformly rotating states, as well as a heteroclinic cycle.[9,10] We observe these states close to the right edge of the shaded region of Fig. 7, the very edge of which exhibits the heteroclinic cycle. Figure 10(a) exhibits the evolution of the amplitude and phase of z_{11} and z_{21} for a nonuniformly rotating cell. The periodicity of both the cell shape and angular speed [shown in Fig. 10(b)] suggests that the bifurcation to nonuniform rotation occurs via a Hopf bifurcation, confirming the predictions of the normal form theory. The heteroclinic cycles observed at the rightmost edge of the shaded parameter domain are shown in Fig. 11(a). Figure 11(b) shows the behavior of the phases of the FB coefficients.

To the best of our knowledge our experimental and numerical states are the first observations of cellular parity-broken modes beyond those on one-dimensional interfaces.[23]

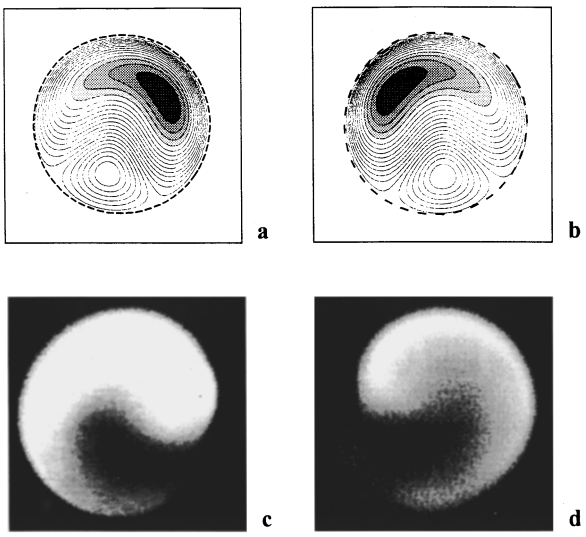

FIG. 8. (a) Clockwise and (b) counter-clockwise rotating states of a single cell from the model, and the analogous states (c) and (d) of the experiment. Observe the qualitative similarity of the cell shape in the two cases. The parameters generating the rotating state are $\eta=2.0$, $\nu_1=0.5$, $\nu_2=1.0$, $B=6.80$ and $R=1.35$.

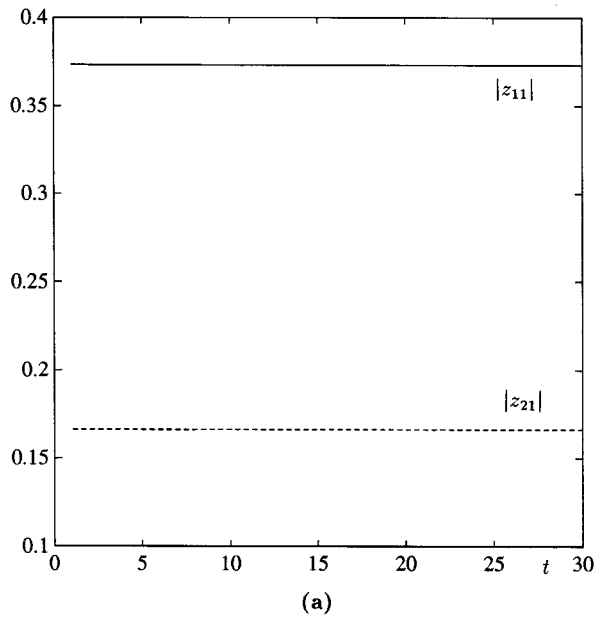

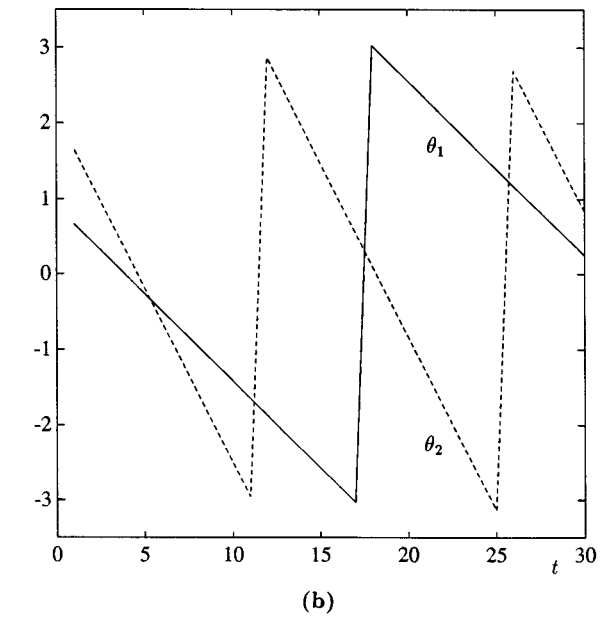

FIG. 9. The evolution of the (a) amplitudes $|z_{11}|$ and $|z_{21}|$ of the primary Fourier–Bessel coefficients, and (b) the corresponding phases, of the cellular state shown in Fig. 8 reveal that it is pure drift mode. The ''phase asymmetry'' $(2\theta_1-\theta_2)$ is constant.

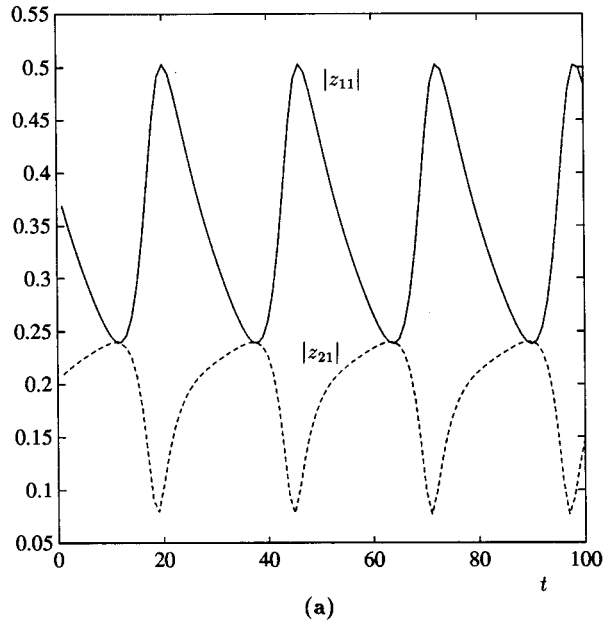

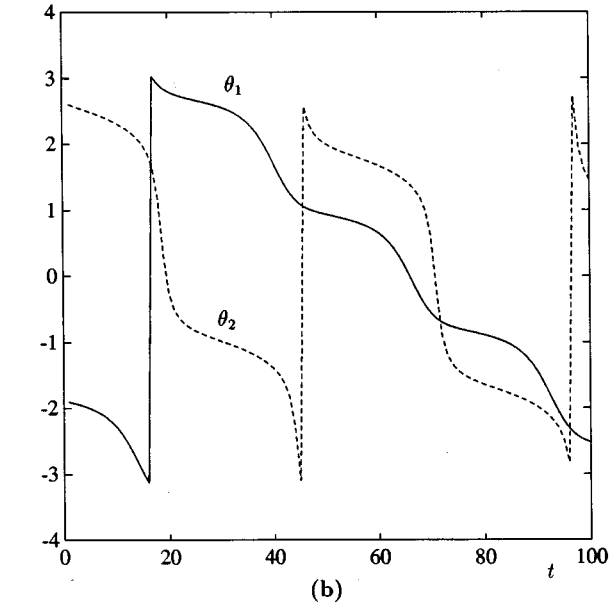

FIG. 10. (a) The evolution of the (a) amplitudes $|z_{11}|$ and $|z_{21}|$ of the primary Fourier–Bessel coefficients, and (b) the corresponding phases, of the nonuniformly rotating cell. The ''phase asymmetry'' $(2\theta_1-\theta_2)$ is a periodic function. The parameters that give this state are the same as Fig. 8, except for $R=1.37$.

Furthermore observations of the nonuniform rotations and heteroclinic cycles resulting from the $k-2k$ mode coupling have not been reported before.

VI. MODAL DECOMPOSITION OF EXPERIMENTAL DATA

For nonstationary patterns, we demonstrate the feasibility of using the Karhunen–Loéve (KL) decomposition to obtain the modes relevant to the dynamics. Karhunen–Loéve decomposition provides an expansion of a given smooth spatiotemporal field $u(\mathbf{x},t)$, in terms of a time-independent orthogonal basis $\{\phi_i(\mathbf{x})\}$ and time dependent amplitudes $\{a_i(t)\}$, such that the reconstruction

$$u(\mathbf{x},t)=\Sigma_i a_i(t)\,\phi_i(\mathbf{x}) \tag{6.1}$$

has a smaller mean-square truncation error than in any other basis.[24–26] The functions $\{\phi_i(\mathbf{x})\}$, determined from the ''data'' $u(\mathbf{x},t)$, are the eigenfunctions of a correlation matrix. The associated eigenvalues λ_i satisfy

$$\langle a_j(t)a_k(t)\rangle=\lambda_j\delta_{jk}, \tag{6.2}$$

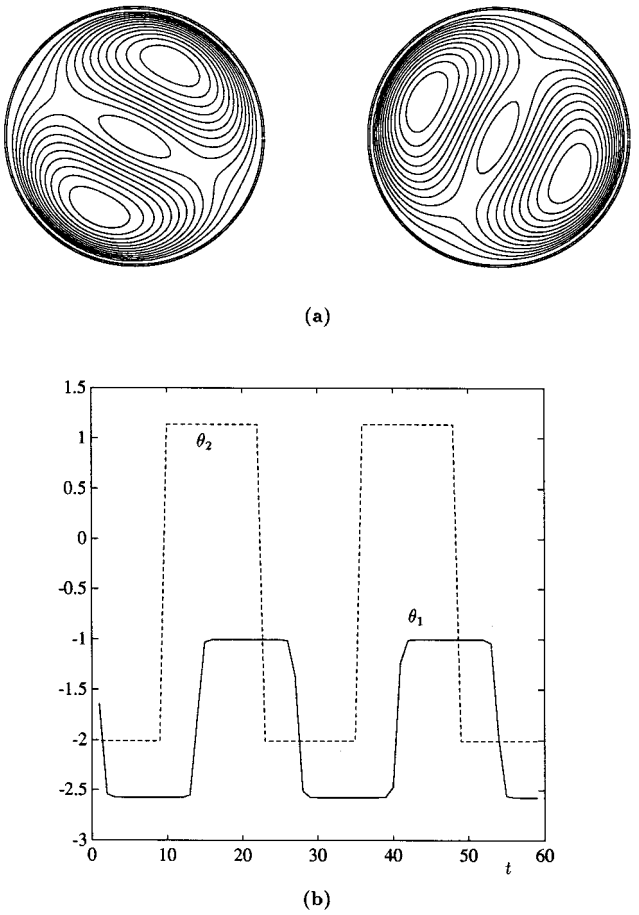

FIG. 11. (a) The two saddle points of a heteroclinic cycle; (b) shows the evolution of the phases of the Fourier–Bessel coefficients z_{11} and z_{21}. The parameters that give this state are the same as Figure 8 except for $R=1.4$.

where $\langle \cdot \rangle$ denotes the time-average operator. λ_j represents the variance of the signal $u(\mathbf{x},t)$ in the direction of the jth eigenfunction. Alternatively, if $u(\mathbf{x},t)$ is considered as a velocity field, then each λ_j represents the average ''kinetic energy'' in the jth mode and $\Sigma\lambda_j$ can be considered to be the total ''energy'' of the data or signal. If the total energy contained in a given truncation of the KL expansion is close to that of the original signal, then the truncated expansion provides a good approximation of the original spatiotemporal ''data.''

The KL modes are estimated from the given spatiotemporal fields; consequently their analytical form, and symmetries are unknown. This precludes us from deducing the normal form equations for the amplitudes of KL modes. Furthermore, the saturation of the intensities of experimental data [see Fig. 1(b)] will result in a proliferation of unphysical KL modes, which can destroy symmetries of the KL modes. We have thus far not succeeded in developing a systematic way to eliminate these problems completely. However, the observation that the combustion front almost vanishes at the boundary suggests that the largest Fourier–Bessel coefficients of a given KL mode may provide information about its symmetries. As shown below, we can identify (with sufficient confidence) the symmetries of the coupled modes, which is the only information needed to deduce the normal form equations.

Figure 12(b) shows the five leading modes from the KL decomposition of the nonuniformly rotating single-cell state, several snapshots of which are shown in Fig. 12(a). These modes capture over 99% of the energy, and give the reproduction shown in Fig. 12(c). The first KL mode, which contains the largest energy, is the time average of the data; it is $O(2)$ symmetric.[27] The next two modes (which can be considered to be the real and imaginary parts of a complex mode analogous to Ψ_{11} of the Fourier–Bessel expansion) are (approximately) D_1 invariant. These pairs of KL modes are combinations of several FB modes of the type Ψ_{1m}. The largest contributions to these come from Ψ_{11}, Ψ_{12} and Ψ_{13}. The phases of these modes are slightly different, leading to the small asymmetry observed in the KL modes. The second pair of modes are approximately D_2 symmetric, and their expansion consists of Ψ_{2m}'s. Ignoring their asymmetry (or taking their largest component in the FB expansion), one can thus deduce the modal decomposition of the rotating states, and the appropriate normal form theory.

Figure 13(a) shows several snapshots of an experimental state with a single rotating cell. Figure 13(b) shows the KL modes with the largest energies, and Fig. 13(c) gives the reconstruction using the first 5 modes. The distinctive asymmetry of the KL modes is due to the phase difference between the different z_{nm}'s for a fixed n. Analysis of artificially saturated data from the model indicates that the cutoff of experimental data [Fig. 1(b)], and the form of boundary conditions play a role in this asymmetry. The behavior of the amplitudes of the KL modes (Fig. 14(a)) can be used to deduce that the rotation is nonuniform. Figure 15 provides the results of the analysis of a rotating state with two cells, and the rotation in this case is seen to be much closer to being uniform (Fig. 14(b)).

Finally, Fig. 16 shows the results from the KL analysis of a cycle between two distinct states. The phase of the (complex) coefficients of the KL modes (Fig. 17) can be used to deduce that the motion corresponds to a heteroclinic cycle.

VII. DISCUSSION

We have used a phenomenological model and bifurcation theory to understand certain aspects of cellular patterns on a flame front. The work is complementary to a detailed numerical study of simplified models of a flame front, e.g., the Kuramoto–Sivashinsky equation. Our work aims to determine the general features such as the existence of rings of cells and the relationships between distinct patterns observed in the experiments. It was shown through several examples that certain features of both stationary and dynamic patterns can be deduced using the appropriate theories of mode-coupling.

The essential first step in the analysis is the identification of the modes whose coupling leads to interesting patterns. We have shown how states consisting of rings of cells can be established. Furthermore, we are able to deduce (observable)

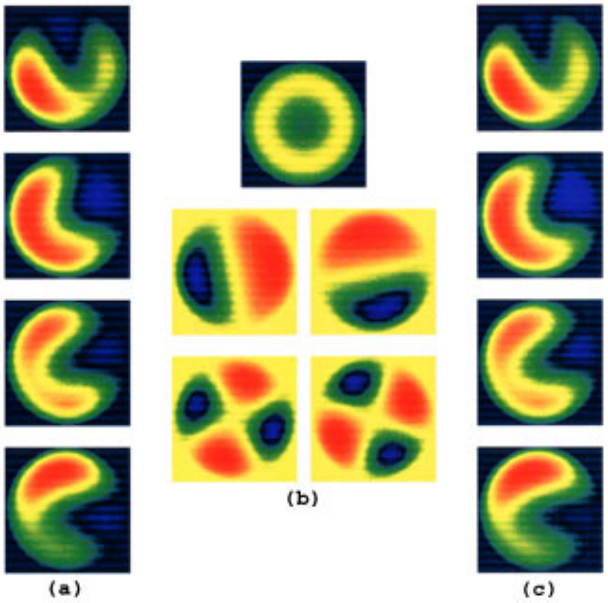

FIG. 12. The Karhunen–Loéve analysis of a single nonuniformly rotating cell generated in the model (3.1): (a) shows several snapshots of the state, demonstrating the shape changes of the cell. The five largest KL modes are shown in (b). The first is the mean value of the field. The next two pairs of KL modes are analogous to the real and imaginary parts of the FB functions Ψ_{11} and Ψ_{21} (the former is well approximated by a linear combination of Ψ_{11}, Ψ_{12} and Ψ_{13}, while the latter is approximated by a linear combination of Ψ_{21}, Ψ_{22}, Ψ_{23} and Ψ_{24}). The reproduction using these five KL modes is given in (c).

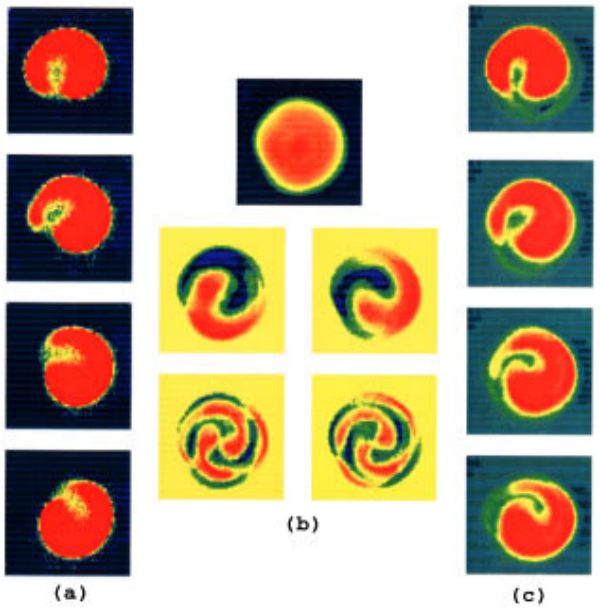

FIG. 13. The Karhunen–Loéve decomposition of a single nonuniformly rotating cell from the experiment. The layout is similar to that of Fig. 12. The distinctive asymmetry of the KL modes is due to the phase difference between the FB coefficients. This is in part due to the saturation of the experimental data.

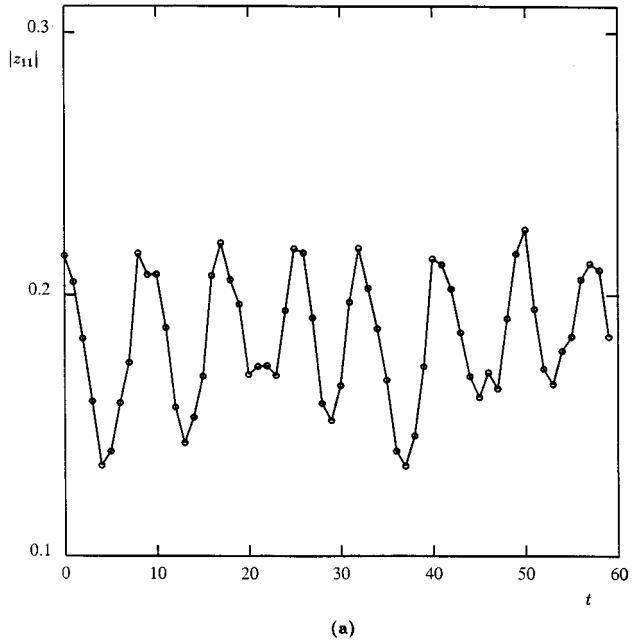

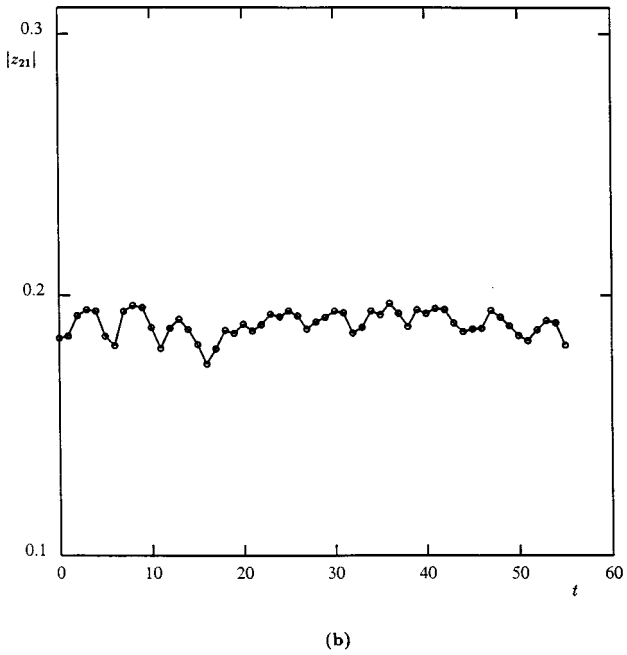

FIG. 14. The evolution of the amplitude of primary KL mode for (a) rotating single cell state shown in Fig. 13, clearly showing the periodic modulations, and hence that the rotation is nonuniform. In contrast (b), which shows the amplitude of a primary KL mode of the rotating two-cell state shown in Fig. 15, indicates that the rotation is uniform.

properties of nonstationary states. In Sections IV–VI and the Appendix, we have presented aspects of this analysis. Properties of cellular flame patterns appear to be intimately related to the orthonormal expansion appropriate to a circular domain, i.e., the Fourier–Bessel expansion.[17,28] However, the patterns observed are not pure FB modes, but rather their combinations. The subcriticality of the primary bifurcations, and the presence of the gradient terms in the model explain

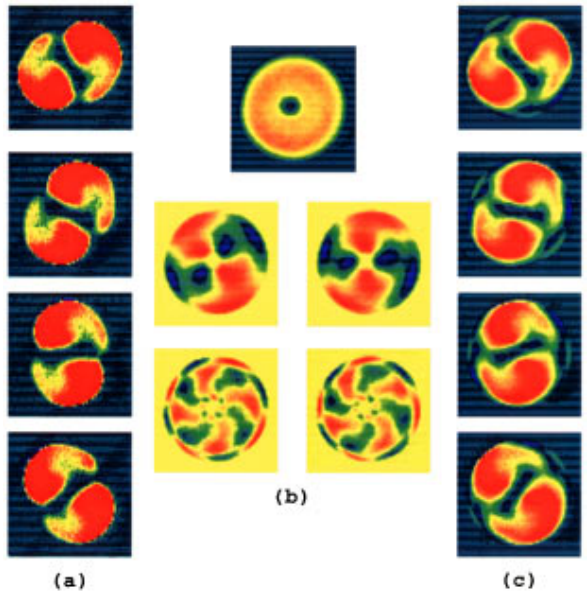

FIG. 15. The Karhunen–Loéve decomposition of a rotating state with two cells. The layout is similar to that of Figs. 12 and 13. A good approximation of these KL modes require about a dozen FB modes.

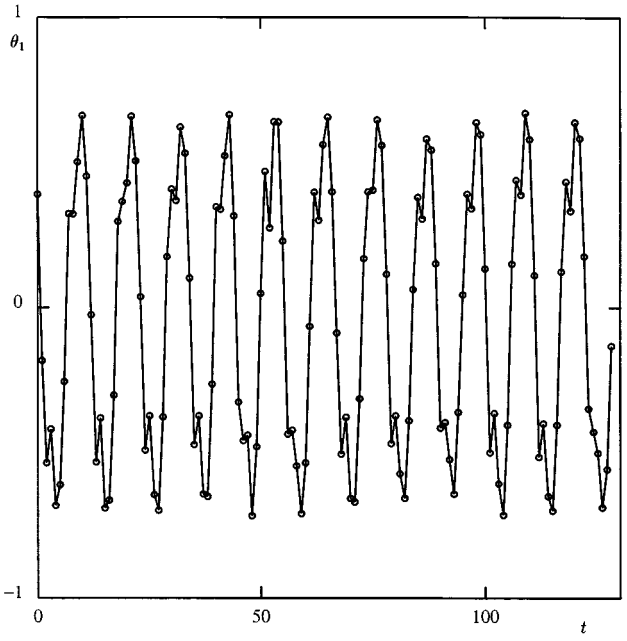

FIG. 17. The phase of the KL modes for the heteroclinic cycle show the motion between two saddle points.

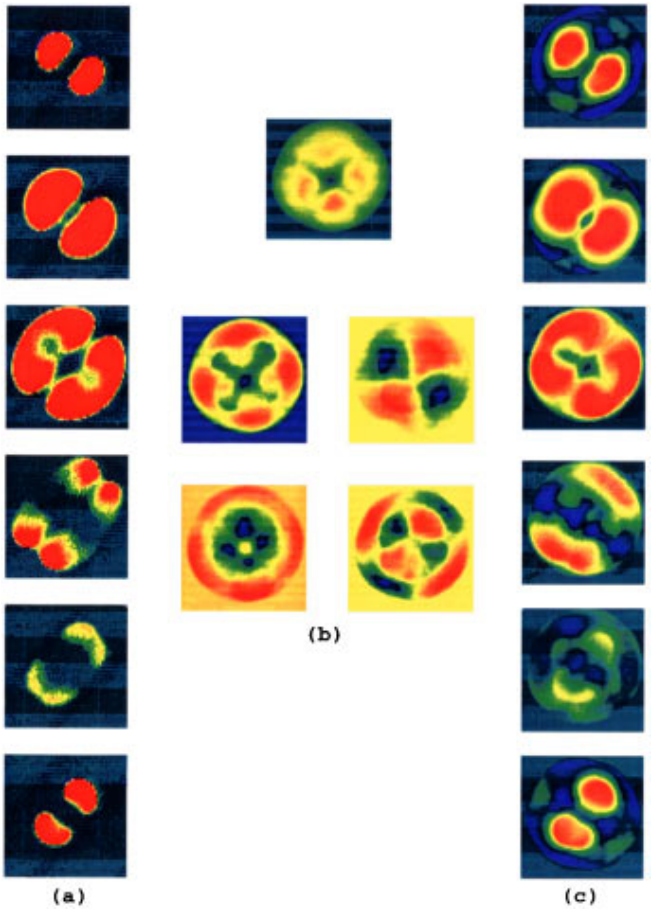

FIG. 16. (a) Snapshots from a heteroclinic cycle moving between two saddle points, (b) the principal modes of the KL decomposition and (c) the reconstruction from these modes.

why this can be the case. The Bessel functions of those FB modes that combine to produce cellular patterns have zeros in close proximity. In states with multiple rings of cells with different symmetries (e.g., Fig. 1), several FB functions contribute to the cells in each ring. The observed weak coupling between distinct rings (as is observed in ratcheting states[4] where the inner ring rotates intermittently without affecting the outer ring significantly) is also explained through the proximity of roots of the Bessel functions. What is clear is that the explanation of the origin of these features does not lie in a microscopic theory of the flame front.

The introduction of a (numerically) integrable phenomenological model allows a comprehensive analysis of many stationary and nonstationary states, including a study of the effects of noise and those of boundary conditions. Stability domains of distinct states can be obtained with greater accuracy; in particular, we have been able to locate nonuniform rotating states and the heteroclinic cycles predicted by the normal form theory. The ability to analyze experimental patterns through Karhunen–Loéve analysis complements these results. To the best of our knowledge, nonuniform rotating states and heteroclinic cycles of the type discussed have not been shown to be present in experiments before. In future work, the KL decomposition will be used to derive low-dimensional approximations to the KS equation.[29]

We conclude with a brief demonstration of the advantages provided by a modal analysis in the study of more complex nonstationary states. Figures 18(a) and 18(b) show snapshots from the ''hopping state,'' where three cells in a single ring rotate with nonuniform angular speed. The dynamics and the evolution of cell shapes appears to be quite complex and distinct for each cell; the trailing cell changes its shape more than the other two.[2] Fourier–Bessel decom-

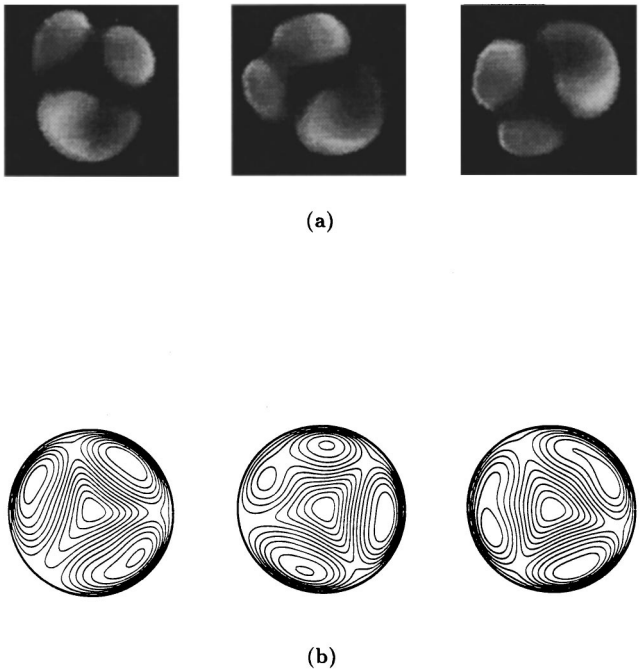

FIG. 18. Hopping modes seen in the (a) experiment and (b) the model (3.1). Observe that the cell shapes and angular velocities appear to change in a complicated way. However a Fourier–Bessel decomposition of these states unravels this complexity, and provides the modes essential to study the dynamics.

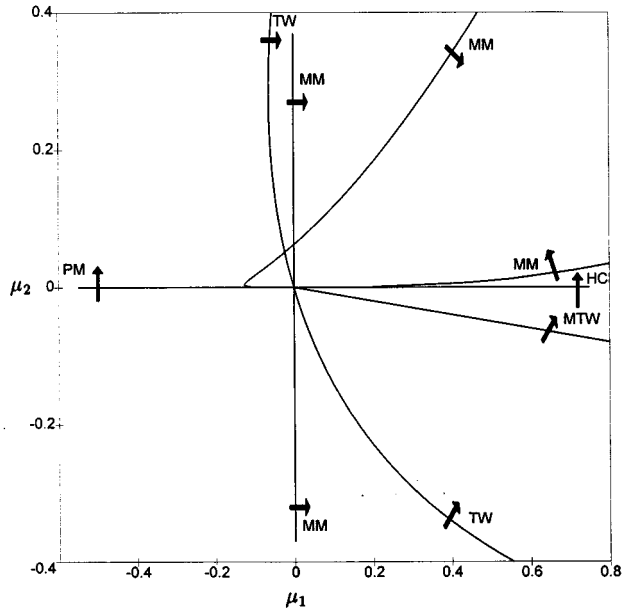

FIG. 19. The bifurcation set for Eq. (A2). The trivial state $(u,v)=(0,0)$ is stable for $\mu_1<0$ and $\mu_2<0$. Along the line $\mu_2=0$ the uniform state undergoes a bifurcation to Ψ_{21} which is chosen to be degenerate. The bifurcation across $\mu_1=0$ leads to a mixed mode which remains supercritical. TW, MTW and HC show bifurcations to traveling modes, modulated traveling modes, and heteroclinic cycles respectively. The parameters $e_{11}=-1$, $e_{12}=-2$, $e_{21}=-1$, $e_{22}=0$ and $e_{23}=-1$ are fixed.

position of the numerically generated state unravels most of the complexity of the dynamics and reveals that the primary modes excited, Ψ_{12}, Ψ_{31} and Ψ_{41}, undergo periodic motion. Not surprisingly, the zeros α_{12}, α_{31} and α_{41} are close to each other and thus the modes can be simultaneously excited.

In order to develop the normal form analysis we need to deduce a representation of the invariances in terms of the coefficients z_{12}, z_{31} and z_{41} of the Fourier–Bessel series. Rotations are represented by $(z_{12},z_{31},z_{41}) \rightarrow (z_{12}e^{i\theta},z_{31}e^{3i\theta},z_{41}e^{4i\theta})$ while reflections are represented by $(z_{12},z_{31},z_{41})\rightarrow(\bar{z}_{12},\bar{z}_{31},\bar{z}_{41})$. Observe that the normal form depends only on the azimuthal index of the Fourier–Bessel functions, while the ''radial'' part $J_{nm}(\alpha_{nm}r/R)$ determines the modes Ψ_{nm} that can be excited simultaneously. Unlike the rotating states studied in Section V, the coupling of modes leading to hopping states would not be expected in one dimensional problems. The analysis of the normal form will be presented elsewhere.[29]

ACKNOWLEDGMENTS

Dr. M. el-Hamdi made the initial observations on rotating and hopping states, and Alfredo Martinez carried out early numerical integrations of the model (3.1). We have benefited greatly from many discussions with Mike Field, Martin Golubitsky, Victor LeBlanc, Bernie Matkowsky and Ian Melbourne. This work is partially funded by the Office of Naval Research through Grant Nos. N-00014-K-0613 and N-00014-94-1-0949. The programs KL-TOOL and AUTO were used to obtain Karhunen–Loéve analysis and the bifurcation sets reported here.

APPENDIX: NORMAL FORM ANALYSIS

A brief description of the normal form analysis corresponding to the $k-2k$ mode coupling will be provided in the Appendix.[5,9,10] The primary bifurcations for our model (as well as for the experimental system) are subcritical, see Fig. 7. Consequently, earlier analyses of the mode coupling, though providing an insight to the possible bifurcation sets, are not strictly applicable here. However, the nonstationary states observed in the model (i.e., uniform rotation, nonuniform rotation, and heteroclinic cycles) suggest that the bifurcation sets are similar in the two cases. We present the mode-coupling theory for the case when the primary bifurcations (to Ψ_{11} and Ψ_{21}) are degenerate.[5] Unfolding of the degeneracy (leading either to subcritical or supercritical transitions) will preserve the bifurcation diagram. The analysis of the degenerate case will thus not only explain our results, but will also suggest why the observed states are similar in the two cases.

The normal form equations are equivariant under rotations by an arbitrary angle θ and reflections. Using the FB coefficients, these operations are represented by $(z_{11},z_{21})\rightarrow(z_{11}e^{i\theta},z_{21}e^{2i\theta})$ and $(z_{11},z_{21})\rightarrow(\bar{z}_{11},\bar{z}_{21})$ respectively. Equations that are equivariant under the operations take the form[30]

$$\dot{z}_{11}=P_1(I_1,I_2,I_3)z_{11}+Q_1(I_1,I_2,I_3)z_{21}\overline{z}_{11},$$
$$\dot{z}_{21}=P_2(I_1,I_2,I_3)z_{11}+Q_2(I_1,I_2,I_3)z_{11}^2, \tag{A1}$$

with $I_1=|z_{11}|^2$, $I_2=|z_{21}|^2$, and $I_3=z_{21}\overline{z}_{11}^2+\overline{z}_{21}z_{11}^2$. Using the lowest order required to provide the degeneracy of the primary bifurcations give

$$\dot{z}_{11}=\overline{z}_{11}z_{21}+z_{11}(\mu_1+e_{11}|z_{11}|^2+e_{12}|z_{21}|^2),$$
$$\dot{z}_{21}=-\overline{z}_{11}^2+z_{21}(\mu_2+e_{21}|z_{11}|^2+e_{22}|z_{21}|^2+e_{23}|z_{21}|^4). \tag{A2}$$

The uniform state $(z_{11},z_{21})=(0,0)$ is stable for $\mu_1<0$ and $\mu_2<0$. Across $\mu_2=0$, there is a bifurcation to *pure modes* ($\Psi_{21}(r,\theta)$ in our case) which lie on the invariant subspace $z_{11}=0$. For this bifurcation to be degenerate e_{22} has to be chosen to be 0. Figure 19 shows the bifurcation set for a particular choice of the remaining parameters, showing the existence of (1) the bifurcations to rotating states, (2) the secondary Hopf bifurcations to modulated rotating states, and (3) bifurcations to the heteroclinic cycles. These bifurcations were also observed in the model, see Fig. 7.

[1] M. Gorman, F. Hamill, M. el-Hamdi, and K. Robbins, Combust. Sci. Technol. **98**, 25 (1994).
[2] M. Gorman, M. el-Hamdi, and K. Robbins, Combust. Sci. Technol. **98**, 71 (1994).
[3] M. Gorman, M. el-Hamdi, and K. Robbins, Combust. Sci. Technol. **98**, 79 (1994).
[4] M. Gorman, B. Pearson, M. el-Hamdi, and K. A. Robbins, Phys. Rev. Lett. **76**, 228 (1996).
[5] M. Golubitsky, I. Stewart, and D. G. Schaeffer, *Singularities and Groups in Bifurcation Theory* (Springer-Verlag, New York, 1988), Vol. 2.
[6] B. L. Keyfitz, M. Golubitsky, M. Gorman, and P. Chossat, Lect. Appl. Math. **24**, 293 (1986).
[7] G. H. Gunaratne, M. el-Hamdi, M. Gorman, and K. A. Robbins, Mod. Phys. Lett. B **10**, 1379 (1996).
[8] S. Rosenblat, S. H. Davis, and G. M. Homsy, J. Fluid. Mech. **120**, 91 (1982).
[9] G. Dangelmayr, Dynam. Stability Syst. **1**, 159 (1986).
[10] D. Armbruster, J. Guckenheimer, and P. Holmes, Physica D **29**, 257 (1988).
[11] M. R. E. Proctor and C. A. Jones, J. Fluid Mech. **188**, 301 (1988).
[12] G. I. Sivashinsky, Acta Astronaut. **4**, 1177 (1977); Y. Kuramoto, Prog. Theor. Phys. Suppl. **64**, 346 (1978).
[13] S. B. Margolis and B. J. Matkowsky, Combust. Sci. Technol. **34**, 45 (1983).
[14] J. M. Hyman and B. Nicolaenko, Physica D **18**, 113 (1986).
[15] I. Prigogine and R. Lefever, in *Membranes, Dissipative Structures, and Evolution*, edited by G. Nicholis and R. Lefever (Wiley, New York, 1974).
[16] W. H. Press, B. P. Flannery, S. A. Teukolsky, and W. T. Vettering, *Numerical Recipes—The Art of Scientific Computing* (Cambridge University Press, Cambridge, 1988).
[17] G. Watson, *A Treatise on the Theory of Bessel Functions* (Cambridge University Press, Cambridge, 1962).
[18] The values of γ_1 and γ_2 are 5.21659 and 0.82582 respectively.
[19] W. S. Edwards and S. Fauve, J. Fluid Mech. **278**, 123 (1994).
[20] J. Gollub (private communication).
[21] A. J. Simon, J. Bechhoefer, and A. Libchaber, Phys. Rev. Lett. **61**, 2574 (1988); G. Faivre, S. de Cheveigne, C. Guthmann, and P. Kurowski, Europhys. Lett. **9**, 779 (1989); M. Rabaud, S. Michalland, and Y. Couder, Phys. Rev. Lett. **64**, 184 (1990); F. Daviaud, M. Bonnetti, and M. Dubois, Phys. Rev. A **42**, 4338 (1990).
[22] P. Coullet, R. E. Goldstein, and G. H. Gunaratne, Phys. Rev. Lett. **63**, 1954 (1989); R. E. Goldstein, G. H. Gunaratne, L. Gil, and P. Coullet, Phys. Rev. A **43**, 6700 (1991).
[23] Rotating cells have been observed in a quasi-one-dimensional model, see A. Bayliss, B. J. Matkowsky, and H. Riecke, in *Numerical Methods for PDEs with Critical Phenomena*, edited by H. Kaper and M. Garbey (Kluwer, Dordrecht, 1994). They have also been recently observed in a detailed model of flame fronts (A. Bayliss and B. J. Matkowsky, private communication).
[24] L. Sirovich, Q. Appl. Math. **XLV 3**, 561 (1987).
[25] G. Berkooz, P. Holmes, and J. L. Lumley, Annu. Rev. Fluid Mech. **25**, 115 (1993).
[26] D. Armbruster, R. Heiland, and E. Kostelich, Chaos **4**, 421 (1994).
[27] M. Dellnitz, M. Golubitsky, and M. Nicol, *Symmetry of Attractors and the Karhunen–Loéve Decomposition* in Trends and Perspectives in Applied Mathematics, edited by L. Sirovich (Springer-Verlag, New York, 1994), p. 73.
[28] M. Golubitsky, E. Knobloch, and I. Stewart, ''Target Patterns and Spirals in Planar Reaction-Diffusion Systems,'' University of Houston preprint.
[29] A. Palacios, G. H. Gunaratne, M. Gorman, and K. A. Robbins (unpublished).
[30] E. Buzano and A. Russo, Ann. Math. Pura Appl. (IV) **146**, 217 (1987).